# CHARACTERIZATION OF SOME RHENIUM INCONEL SUPERALLOYS MADE IN A VACUUM INDUCTION FURNACE AND CAST IN ARGON ATMOSPHERE

Andrei Constantin BERBECARU[1], George COMAN[1*], Sorin CIUCĂ[1], Andrei GRECU[1], Ioana Arina GHERGHESCU[1], Mihai DOBRE[1], Mirela SOHACIU[1], Ecaterina MATEI[1], Andra Mihaela PREDESCU[1], Ionela-Alina DIACONU[1], Cristian PREDESCU[1]

*The paper presents some particularities of the manufacturing in the vacuum induction furnace and the argon atmosphere of three Ni – base Inconel - like superalloys. As a novelty, besides the typical alloying elements, the alloys contain rhenium between 1 and 3%. By means of optical and scanning electron microscopy/energy-dispersive X-ray spectrometry (SEM-EDS), the compositional and microstructural differences after casting were analyzed. The alloy that contains the smallest amount of Re, but also Mo, has a structure that reveals a lesser dendritic segregation, creating favorable premises for subsequent processing and also a high refractoriness.*

**Keywords**: Inconel, superalloys, rhenium

## 1. Introduction

Nickel-based superalloys (Inconel) are very complex, widely used for parts working at high temperatures. Specifically, they are used in the manufacture of commercial and military aircraft gas turbines, power generators or marine propulsion technology. Superalloys also have important applications in the oil and gas industry, space vehicles, submarines, nuclear reactors, military electric motors, chemical processing vessels, and heat exchanger tubes [1]. Several generations of superalloys have been developed, each generation tending to have higher high temperature strength [2]. The latest generations of Ni base superalloys contain rhenium (Re), a refractory alloying element which improves the high temperature mechanical properties [3].

The alloying elements present in the chemical composition of the three Inconel superalloys developed for experimentation - Al, Nb, Mo, Ti, Co, Ta, W, Re - were chosen in such a way as to ensure the necessary technological characteristics, primarily related to a good machinability, but also to improve the working characteristics at high temperatures.

Thus, molybdenum is added to improve the corrosion and high temperature resistance of Inconel alloys. Titanium and niobium are added to improve

[1] National University of Science and Technology POLITEHNICA Bucharest, Romania, e-mail: contact authors' e-mail: george.coman@upb.ro

mechanical properties by precipitation of phases that enhance the dispersion hardening mechanism and aluminum is added in order to improve thermal stability and corrosion resistance. Aluminum also has a favorable effect in the alloy making process, being one of the best deoxidizers and degasifiers [4, 5]. The rhenium addition in the chemical composition will increase the stability at high temperatures, rhenium itself being a refractory element. Moreover, rhenium determines the improvement of creep resistance, a very important characteristic for mechanical parts that work at high temperatures [6]. Rhenium also confers a sustainable corrosion resistance of Inconel alloys in chemically aggressive environments that frequently change their basic character to acid and vice versa, depending on the chemical reactions specific to the engine functioning that take place with fast kinetics at high temperatures [7]. An important structural characteristic of rhenium is that in small quantities and in the presence of nickel it does not form compounds, it is distributed by substitution in nickel-based solid solutions [8, 9]. In larger quantities, it would be found in intermetallic compounds with hardening phases role. However, this role will be ensured by other alloying elements intentionally chosen for this purpose.

## 2. Materials and experimental methods

This research studied three types of nickel-based superalloys containing 1%, 2% and 3 wt% rhenium. The choice of the rhenium amount of was judiciously established. Rhenium is an expensive and scarce element, so the quantity must be chosen economically. Secondly, the structural effect that small amounts of rhenium plays in Inconel alloys, when it is only found dissolved in the solid solution, was taken into account.

The alloys were made in a vacuum induction furnace with a controlled atmosphere of the Five CELES type (model ALU 600). By using this type of furnace, the aim was to eliminate possible contamination and oxidation of the metallic melt, casting in structural and batch composition homogeneity conditions, as well as directional solidification of the alloys.

Two already known Ni – base superalloys with Re (2 wt% and 3 wt%) [10] and one superalloy with Re of a new composition, with 1 wt% Re, were made. The refractoriness characteristics improve with the increase of Re content, being directly related to the alloy melting temperature. The presence of Al increases the high temperature oxidation resistance. The percentages of Cr and Mo were increased and the percentages of W and Ta were decreased. The compositions of these superalloys are shown in Table 1.

*Table 1*

**Chemical composition of the Inconel alloys (wt%)**

| Alloy | Ni (%) | Cr (%) | Co (%) | Al (%) | Ta (%) | Mo (%) | Fe (%) | W (%) | Re (%) | Ti (%) | Nb (%) | C (%) |
|---|---|---|---|---|---|---|---|---|---|---|---|---|

| | | | | | | | | | | | | |
|---|---|---|---|---|---|---|---|---|---|---|---|---|
| **Alloy 1 (S1)** | 63,04 | 6,92 | 9,87 | 5,20 | 6,58 | 0,58 | - | 4,34 | 1,96 | 1,49 | - | 0,02 |
| **Alloy 2 (S2)** | 60,06 | 6,47 | 9,61 | 8,27 | 6,27 | 0,56 | - | 4,31 | 2,98 | 1,45 | - | 0,02 |
| **Alloy 3 (S3)** | 64,28 | 12,62 | 5,89 | 5,43 | 3,38 | 2,71 | 1,76 | 1,28 | 1,02 | 0,79 | 0,76 | 0,03 |

The composition of the Ni – base superalloys was chosen taking into account the influence of each alloying element on the physical-mechanical properties, especially on the corrosion resistance at high temperatures.

The new Ni – based alloys manufacturing in an argon atmosphere allowed the melt to be protected during their melting in a copper crucible. The as-cast rods were of 20 mm in diameter. The materials used for the alloy manufacturing were preheated to 250 °C.

The obtained samples were prepared for the metallographic examination and for the hardness tests, as follows: a cylindrical portion, called a sample, of approximately 5 mm height was cut from each ingot. A Struers preparation line was used; the samples were embedded in resin, polished and etched with Marble reagent to highlight the structure; then they were examined using an Olympus type metallographic microscope (BX 51 M), equipped with the possibility of investigations in bright or dark field and magnifications up to 1000x.

The purpose of these investigations was to determine the hardness values after processing and casting and to observe the structure obtained directly after casting, with all the effects induced by the specific transformations that take place during processing in the vacuum induction furnace, argon atmosphere and cooling directed.

## 3. Results

### 3.1. Alloys hardness after casting

The hardness values of the Inconel superalloys after casting, measured with the Innovatest Falcon 500 automatic hardness tester, are presented in Table 2.

*Table 2*

**Hardness values of the Inconel superalloys after casting**

| *Alloy* | *Hardness (HV2)* | *Average Hardness (HV2)* |
|---|---|---|
| *S1* | *428* | *428* |
| | *398* | |
| | *436* | |
| | *426* | |
| | *451* | |
| *S2* | *454* | *445* |
| | *454* | |
| | *443* | |
| | *441* | |
| | *433* | |
| *S3* | *417* | *416* |

| | | |
|---|---|---|
| | 419 | |
| | 426 | |
| | 412 | |
| | 405 | |

One may see that the hardnesses for sample 1 fall between 328 and 451 HV2 with an average value of 428 HV2, sample 2 records values between 433 and 454 HV2 with an average value of 445 HV2 and sample 3 shows hardness values between 405 and 417 HV2, the average value being 416 HV2.

A first observation is related to the increase of the alloying degree; consequently, the mechanical resistance performance represented by the hardness value also increases. Obviously, these data cannot be considered as a final conclusion; only the final heat treatments will decide the mechanical performances.

A second observation refers to the fact that the set of hardness values recorded for each sample demonstrate quite close numbers to each other, suggesting a fairly high homogeneity from a chemical and structural point of view. This represents a very important positive argument for the new technique of making and casting Inconel alloys. However, the information will be properly verified with specific methods of structural and compositional characterization.

## 3.2. Metallographic analysis of the samples obtained by vacuum induction furnacemaking in cold crucible and casting in argon atmosphere.

### 3.2.1. Structural analysis by optical microscopy

Figs. 3, 4 and 5 show the analyzed optical microscopy images of the three samples.

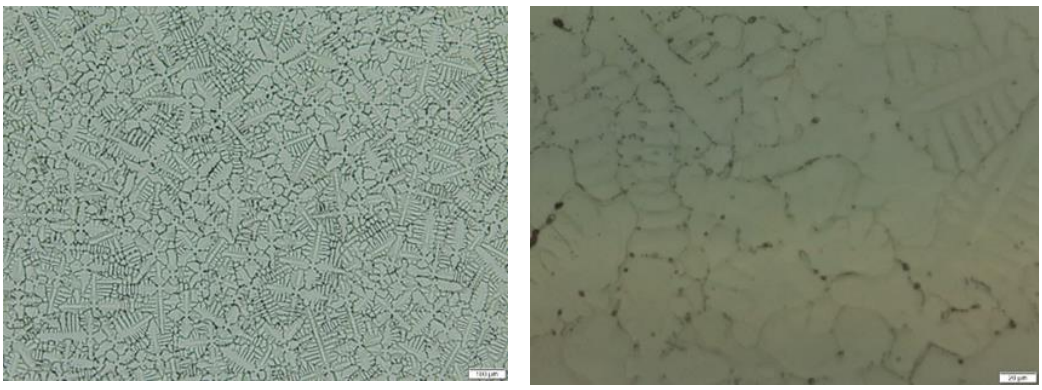

a) b)

Fig. 3. Optical micrographs of sample S1, Marble reagent, a) M = 100x; b) M = 500x;

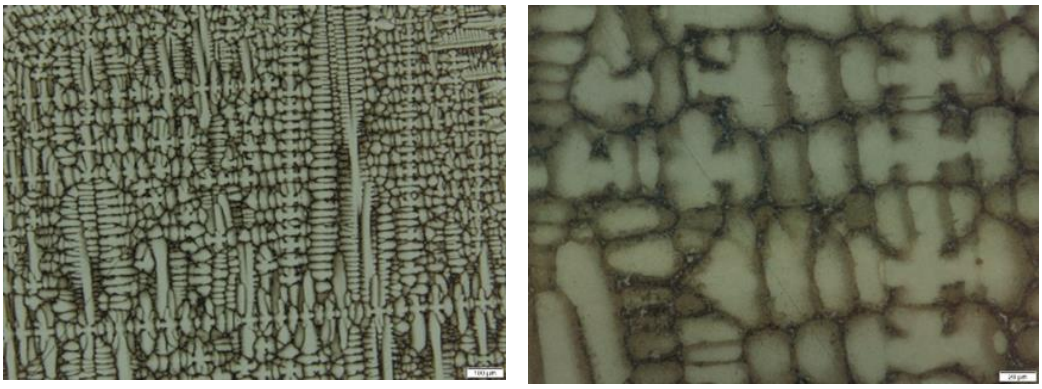

a) b)

Fig. 4. Optical micrographs of sample S2, Marble reagent, a) M = 100x; b) M = 500x;

The purpose of these investigations was to observe the structure obtained directly after casting, with all the effects induced by the phenomena that take place during the making in the vacuum induction furnace, casting in argon atmosphere and directional cooling.

The microstructures were analyzed both at low magnification (M = 100x) to have an overview of the structure, and also at higher magnification to observe certain important structural details.

Next, the microscopic analysis for samples S1 and S2 will be performed in parallel, the samples having many similarities. They have in common the fact that in their chemical composition the proportion of high melting point elements (Re, W, Ta) progressively increases. The result consist in obtaining structures with high chemical and structural inhomogeneity, represented by the massive appearance of dendritic formations. Their density and development increases from sample S1 to S2, together with the proportional increase of the mentioned elements, proving that the degree of undercooling $\Delta T_r$ specific to the manufacturing process was very high.

If in sample S1 the dendrites of the γ solid solution are finer, with the main dendrite axis being shorter, in sample S2 the dendrites are very well outlined, even coarse. Their orientation is done in well-defined directions, retracing the elimination direction of the thermal flow during cooling.

The image at higher magnification (b) captures, especially in the case of sample S1, the existence of some porosities (dark areas) in the dendrites boundaries, as a result of the capillarity effect that appeared in the solidification second stage when the liquid phase has lost its fluidity and was no longer able to fill the interdendritic space.

Besides these structural details, fine and bright particles with regular geometry can be observed at the grain boundaries in both samples (S1 and S2) that can be ascribed to primary carbides. One may see also thicker, brown areas, which

represent secondary phases solid state precipitates. Their nature cannot be precisely established.

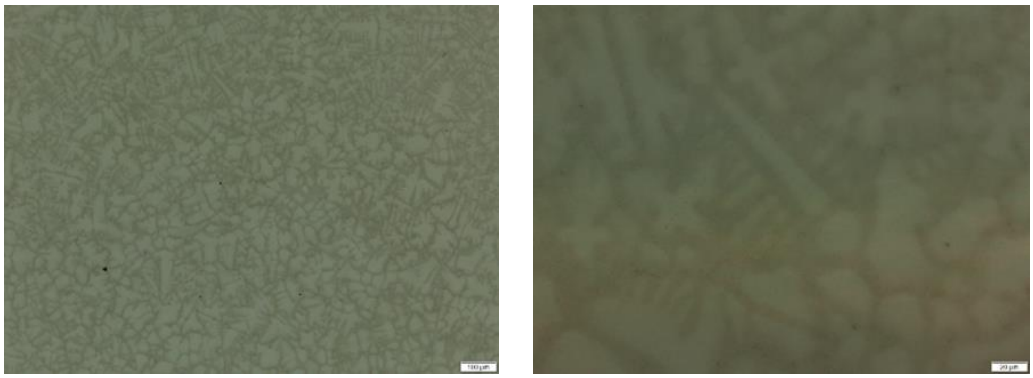

a) b)

Fig. 5. Optical micrographs of sample S3, Marble reagent, a) M = 100x; b) M = 500x;

Sample S3, with the newly proposed, more economical chemical composition, brings a more distinctive structure after solidification. The degree of homogeneity is higher, without excluding the dendritic formations, which are more clearly visible at higher magnifications. A finer grain is observed compared to the other investigated samples.

Correlating these data with the chemical composition of the alloy one can conclude that the higher homogeneity is the consequence of the decrease in quantities of high melting point elements (Re, W, Ta), which caused the degree of undercooling $\Delta T_r$ to be lower. As for the fine - grained structure, this can be attributed to the presence of Mo, an element known for having such an influence [11].

### 3.2.2. Structural and compositional analysis by scanning electron microscopy (SEM) associated with energy dispersive X-ray spectrometry (EDS)

More thorough informations on the structure and local chemical composition of the samples can be obtained by scanning electron microscopy associated with energy dispersive X-ray spectrometry (EDS).

Fig. 6 shows the electron micrographs of sample S1.

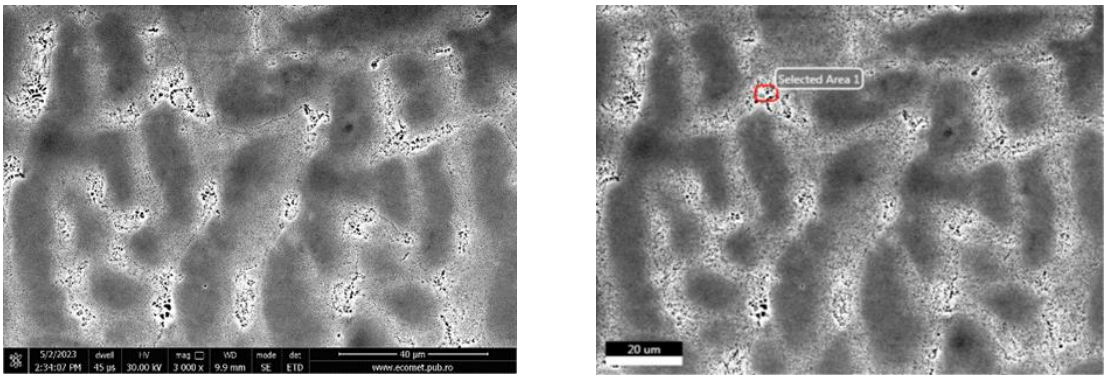


(a) (b)

Fig.6. Scanning electron microscopy (SEM) images of sample S1; a) Secondary electrons image M=3000x; b) Backscattered electrons image with the specification of the area where the EDS compositional analysis was performed

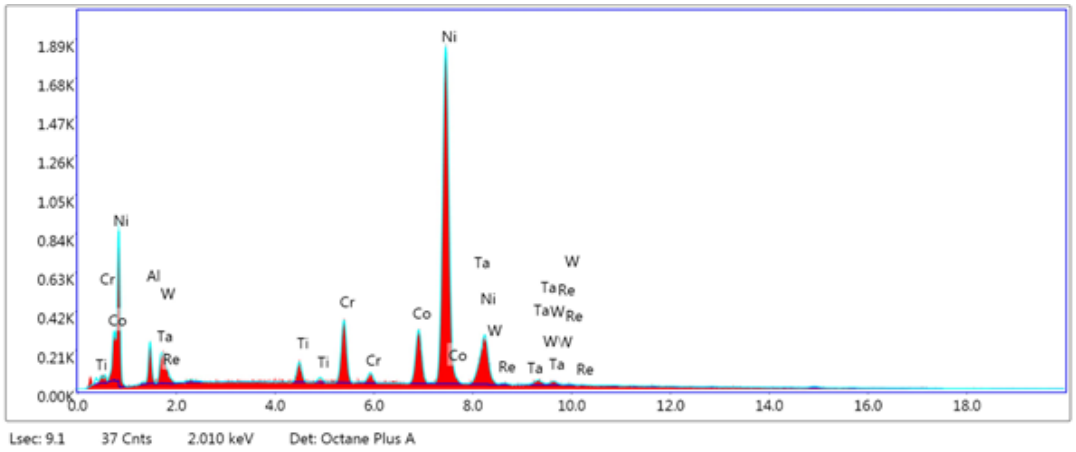


Fig.7. EDS energy dispersive X-ray analysis of sample S1 for the microarea analyzed in Fig. 6 b.

*Table 3*

**Local chemical composition in the selected area from sample S1**

| Chemical element | Wt % | At % |
|---|---|---|
| Al | 7.40 | 15.71 |
| Ti | 1.93 | 2.31 |
| Cr | 6.68 | 7.36 |
| Co | 8.75 | 8.51 |
| Ni | 64.14 | 62.61 |
| Ta | 7.72 | 2.45 |
| W | 2.28 | 0.71 |
| Re | 1.11 | 0.34 |

Some additional information is brought by Fig. 6. The rise in the alloying degree and the percentages of high melting point components lead to an

increasingly marked dendritic aspect. This is easier to observe in electron micrographs than in optical ones, both in the secondary electron image (a) of sample S1, as well as in backscattered electrons image (b).

But the structural detail that brings novelty to the images is the dotted regions clustered in the interdendritic spaces of the γ solid solution. These areas are well delineated in both the secondary electron image and the backscattered electron image. According to the specific morphology, irregularly punctiform, the mentioned formations fall into the category of eutectic-type mechanical mixtures. It is difficult to establish the nature of the phases that form the eutectic, since multicomponent alloys (such as Inconel) should be studied by mathematical modelling on multicomponent diagrams. The only somewhat correct information can be obtained from consulting the binary (of 2 components grouped alternatively) or ternary equilibrium diagrams of the alloy systems that include the studied alloy. The Ni-Cr binary equilibrium diagram shows that at the temperature of 1345 °C an eutectic E ($\gamma_{Ni}+\beta_{Cr}$) is formed. But during the cooling it undergoes transformations, the existing diagram in the specialized literature being drawn as a rule only up to 500 °C. Other researchers [7, 12] mention a binary eutectic E (γ+ γ'), with a formation temperature of around 1300 °C, present in Inconel 718 and Inconel 625 alloys.

Following the chemical analysis in the selected area diffraction of the γ solid solution interdendritic space (Fig. 7, Table 3), one can see that a lower amount of rhenium is found compared to its average composition in the S1 alloy. Thus one may see that rhenium segregates intradendritically. The observation is in agreement with other researchers statements [13]: rhenium is concentrated in the dendrites axes and less in the interdendritic spaces [8].

Fig. 8 shows structural and compositional information of sample S2.

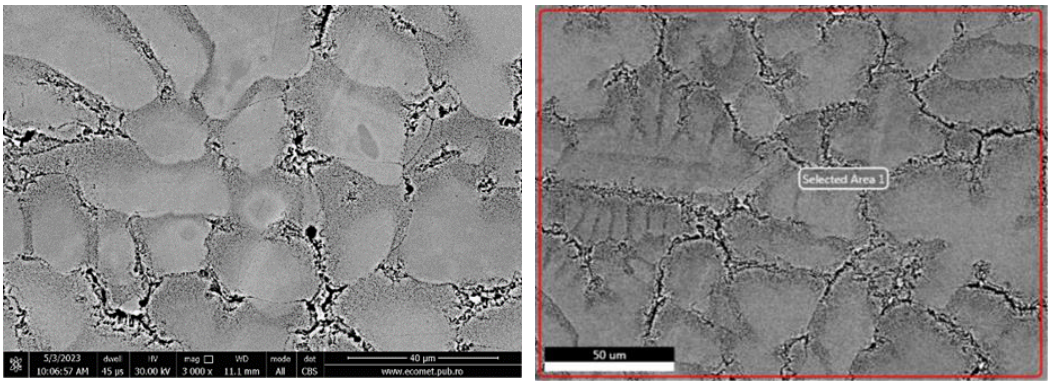


(a) (b)

Fig.8. Scanning electron microscopy (SEM) images of sample S2; a) Secondary electrons image M=3000x ; b) Backscattered electrons image with the specification of the area where the EDS compositional analysis was performed

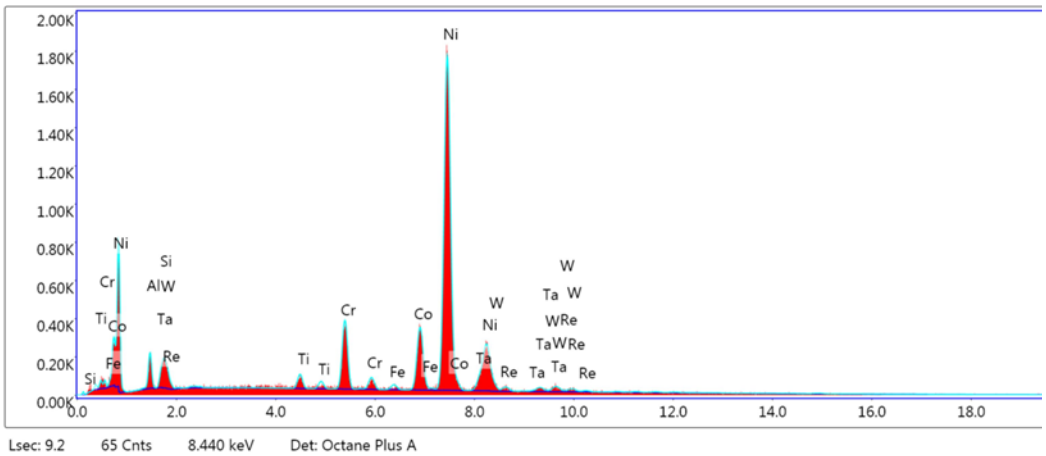


Fig. 9. EDS energy dispersive X-ray analysis of sample S2 for the microarea analyzed in Fig. 8 b.

*Table 4*

**Local chemical composition in the selected area from sample S2**

| Chemical element | Wt % | At % |
|---|---|---|
| Al | 5.71 | 12.62 |
| Ti | 1.33 | 1.65 |
| Cr | 7.20 | 8.27 |
| Fe | 0.60 | 0.64 |
| Co | 9.93 | 10.06 |
| Ni | 61.12 | 62.14 |
| Ta | 6.88 | 2.27 |
| W | 4.64 | 1.51 |
| Re | 2.59 | 0.83 |

The γ solid solution dendritic structure is clearly seen, both in secondary electron images (a) and in backscattered electron images (b). Likewise, the eutectic dotted areas are more extended and grouped towards the grain boundaries, when compared to the previous sample S1.

A structural detail that brings novelty is the presence of the continuous dark formations, distributed at the grain boundaries. According to the morphology, there seem to be phases that are also part of the eutectic composition. They are distributed according to a winding path, following the grain boundaries which themselves have a lacy appearance because it fringes dendritic areas. According to references [4, 5, 7, 8, 14] this morphology is specific to Laves phases, undesirable because they induce fragility.

Another structural aspect found in the microstructures (both *a* and *b*) is represented by the fine dispersion that is concentrated towards the boundaries of the γ solid solution dendrites. These formations belong to the γ' phase [6, 7, 14]. The chemical analysis of the microarea located in the axial zone of a γ solid solution dendrite (Table 6) highlights, among other things, an important amount of rhenium,

which confirms previous research results [8, 9] stating that this element tends to concentrate in the intradendritic zone.

The latest electron microscopy information concerns sample S3 (Fig. 10).

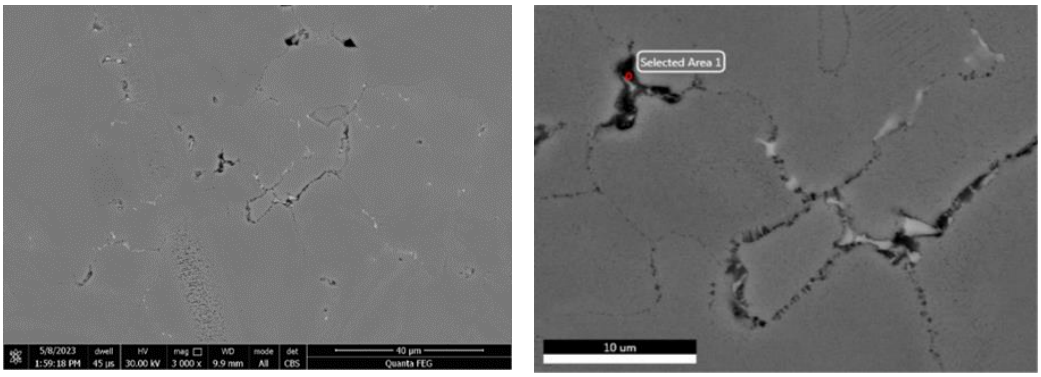


(a) (b)

Fig.10. Scanning electron microscopy (SEM) images of sample S3; a) Secondary electrons image M=3000x; b) Backscattered electrons image with the specification of the area where the EDS compositional analysis was performed.

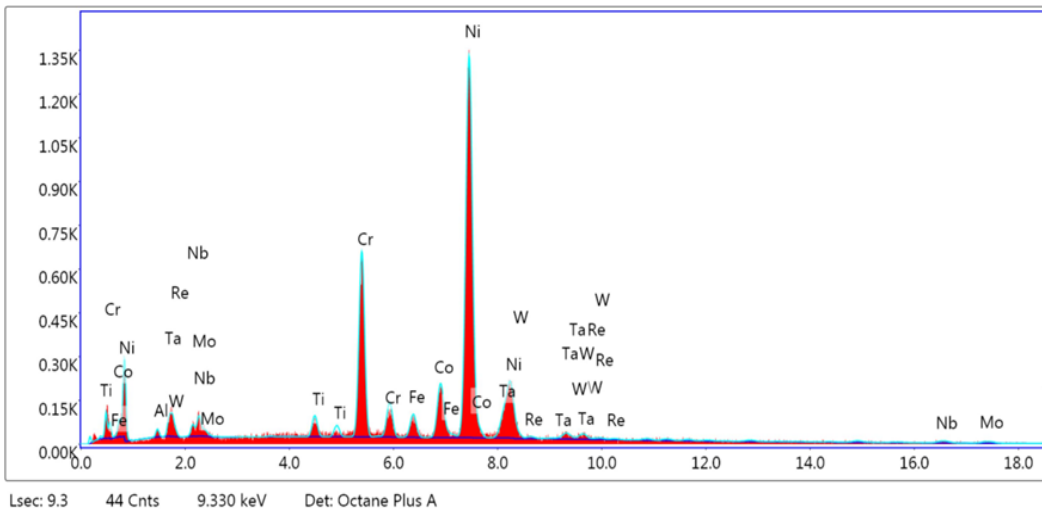


Fig. 11. EDS energy dispersive X-ray analysis of sample S3 for the microarea analyzed in Fig. 10 b.

*Table 5*

**Local chemical composition in the selected area from sample S3**

| Chemical element | Wt % | At % |
|---|---|---|
| Al | 0.87 | 2.09 |
| Ti | 1.41 | 1.91 |
| Cr | 14.47 | 18.15 |
| Fe | 2.12 | 2.47 |
| Co | 6.09 | 6.74 |

| | | |
|---|---|---|
| Ni | 48.68 | 54.10 |
| Ta | 8.08 | 2.91 |
| W | 2.11 | 0.75 |
| Re | 0.84 | 0.29 |
| Nb | 6.53 | 4.58 |
| Mo | 8.81 | 5.99 |

The dendritic aspect of the S3 sample narrows as the amount of high melting point elements in the chemical composition of the alloy decreases. It still persists, as one may see in the optical micrographs, being clearer in the secondary electron image (Fig. 10 a).

At the same time, the eutectic zones shrink significantly. These areas are concentrated at the γ solid solution grain boundaries (where the grains appear more homogeneous). In those microregions, some bright, filiform and quite contorted formations can be identified. Taking into account the previous observations, embrittlement-inducing Laves phases are recognized in this morphology [8, 12].

Other special shapes that can be identified in the image of secondary electrons are those with increased brightness, distributed at the grain boundaries. They can be more clearly seen in backscattered electron images where their regular, polyhedral morphology, specific to primary carbides, also identified in other micrographs, can be observed.

## 4. Conclusions

Alloying with 1% Re will increase the Ni – based alloy high temperature mechanical resistance, Re itself being a refractory element. The novelty consists in the fact that Re, as an alloying element being present in small amounts (1-3%) does not form intermetallic compounds which would unnecessarily consume the available amount of Re needed to ensure a high refractoriness. As foreign atoms in the host lattice, this chemical element is part of a substitutional solid solution, the Ni - based alloy matrix. One may also observe that Re is found in a lesser content inter-dendritically, as against the nominal concentration in all the three studied samples.

The addition of Mo partially compensates for the low concentration of Re, of only 1% in the economical composition alloy, in terms of refractoriness. In addition, it has a positive influence on the grain size refinement, thus ensuring superior mechanical characteristics. The alloying elements being part of the chemical composition of the studied Ni – based alloys (Ta, W, Re) are high melting point elements, which raise the melting temperature of the alloy. Under these conditions, the degree of undercooling $\Delta T_r$ specific to the process becomes higher. The implications on the diffusion phenomena are negative: they are hindered and the structure begins to show an inhomogeneous feature. Following the structural analysis carried out by optical microscopy and scanning electron microscopy, one

may see that all samples have a higher (alloys 1 and 2) or a lower degree (alloy 3) of structural inhomogeneity resulting from solidification. Lower Re, W and Ta contents result in a slightly lower melting point, therefore in a lower degree of undercooling $\Delta T_r$ and also exhibits a lower structural inhomogeneity.

As a general conclusion, the newly created alloy containing 1% Re, presents a reduced chemical inhomogeneity, which will make the further homogenizing annealing to exhibit better results.

**Acknowledgement**

"This work was supported by a grant from the National Program for Research of the National Association of Technical Universities - GNAC ARUT 2023".

## R E F E R E N C E S

[1]. *Tresa M. Pollock, Sammy Tin*, "Nickel-Based Superalloys for Advanced Turbine Engines: Chemistry, Microstructure, and Properties", Journal of Propulsion and Power, **vol. 22**, no.2, 2006, pp. 361-374.

[2]. *D. Locq, P. Caron*, „On some advanced nickel-based superalloys for disk applications". Aerospace Lab, , no. 3, 2011, pp. 1-9.

[3]. *H. Okamoto*, „Ni-Re (Nickel-Rhenium)", J. Phase Equilib. Diffus., **vol. 33**, 2012, p. 346.

[4]. *X. Wang, K. Chou*, „Residual stress in metal parts produced by powder-bed additive manufacturing processes", Proceedings of the 26th Annual International Solid Freeform Fabrication Symposium – An Additive Manufacturing Conference, Austin, Texas, August 10–12, 2015, pp. 1463-1474.

[5]. *H. Zhang, Q. Wang, X. Gong, T. Wang, W. Zhang, K. Chen, C. Wang, Y. Liu, Q. Wang*, „Dependence on temperature of compression behavior and deformation mechanisms of nickel-based single crystal CMSX-4", J. Alloy. Compd., **vol. 866**, 2021, 158878.

[6]. *X. Gong, K. Chou*, „Microstructures of Inconel 718 by selective laser melting", 144th Annual Meeting & Exhibition, Orlando, Florida, 15–19 March 2015, pp. 461-468.

[7]. *A. Strondl, R. Fischer, G. Frommeyer, A. Schneider*, „Investigations of MX and gamma′/gamma″ precipitates in the nickel-based superalloy 718 produced by electron beam melting", Mater. Sci. Eng. A, **vol. 480**, no. 1, 2008, pp. 138-147.

[8]. *Chmiela A., Szczotok B.*, „Effect of Heat Treatment on Chemical Segregation in CMSX-4 Nickel-Base Superalloy", JMEPEG, 2014, **vol. 23**, no. 8, 2014, pp. 2739-2747.

[9]. *Wang B., Zhang J., Huang T., Su H., Li Z., Liu L. Fu H.*, „Influence of W, Re, Cr, and Mo on microstructural stability of the third generation Ni-based single crystal superalloys", Journal of Materials Research, **vol. 31**, no. 21, 2016, pp. 3381-3389.

[10]. Majchrowicz, K., Pakieła, Z., Kamiński, J. *et al.*, „The Effect of Rhenium Addition on Microstructure and Corrosion Resistance of Inconel 718 Processed by Selective Laser Melting", *Metall Mater Trans A*, **vol. 49**, 2018, pp. 6479-6489.

[11]. *A. Hinojos, J. Mireles, A. Reichardt, P. Frigola, P. Hosemann, L.E. Murr, R.B. Wicker*, „Joining of inconel 718 and 316 stainless steel using electron beam melting additive manufacturing technology", Mater. Des., **vol. 94**, no. 8, 2016, pp. 17-27.

[12]. *L.L. Parimi, M.M. Attallah, J.C. Gebelin, R.C. Reed*, „Direct laser fabrication of Inconel 718: effects on distortion and microstructure", Superalloys, 12th International Symposium on Superalloys, Seven Springs, PA, September 09–13, 2012, pp. 511-519.

[13]. *Nageswara Rao Muktinutalapati*, "Materials for Gas Turbines - An Overview", 2011, Advances in gas turbine technology.

[14]. *R.G. Ding, Z.W. Huang, H.Y. Li, I. Mitchell, G. Baxter, P. Bowen*, „Electron microscopy study of direct laser deposited IN718", Mater. Charact., **vol. 106**, 2015, pp. 324-337.